Symmetric transmission electron momentum $(e,2e)$ spectroscopy of an aluminum–aluminum oxide thin foil

P. Hayes, M. A. Bennett, J. Flexman, and J. F. Williams

Department of Physics, The University of Western Australia, Nedlands, Perth, Western Australia 6009, Australia

The experimental mapping of the density of states requires knowledge of all kinematic variables. Conventional techniques, such as photoelectron spectroscopy, average over unobserved variables. The $(e,2e)$ technique, where the scattered and ejected electrons are detected and correlated in time, completely specifies the kinematics. We have successfully applied the technique to thin (130-Å) aluminum (oxide) films with 7.5-keV incident electrons. The use of new position-sensitive detectors on each of the scattered- and ejected-electron-energy analyzers with parallel data collection gives about 2 orders of magnitude improvement in data-collection time over the previous method of sequentially scanning the energy spectrum over a slit. The coincidence binding-energy spectrum with 4.5 eV [full width at half maximum (FWHM)] resolution shows well-defined peaks at 13 and 30 eV which are probably related to the upper and lower valence bands, respectively, of aluminum oxide. This spectrum has been obtained at values of electron momenta from -3.9 to 3.9 Å^{-1} in increments of 0.77 Å^{-1} with a resolution of 1.1 Å^{-1} FWHM. Consideration of the peak dispersion as a function of momentum support the interpretation of an oxide, rather than metallic, origin of the peaks.

I. INTRODUCTION

Aluminum metal has been characterized using many techniques. It exhibits a nearly-free-electron band structure, making it an excellent conductor of heat and electricity. The metal readily oxidizes at its surface forming alumina, a compound which is one of the best known insulators. In everyday applications this two-component system always exists, often mixing in undesirable properties. Surface oxidation under controlled conditions is, however, exploited in metal-oxide-semiconductor (MOS) technology to give insulated-gate devices, as is found for SiO_2. For this reason the mechanics of oxidation in aluminum has been extensively studied by nearly every available surface-analysis method.

Low-energy electron diffraction (LEED), Auger electron spectroscopy (AES), and extended x-ray-absorption fine structure (EXAFS), reviewed, for example, by Batra,[1] have revealed that oxygen is initially chemisorbed onto clean low-index faces of pure aluminum in a disorder overlayer or underlayer, with the exception of the densely packed (111) face. Increasing the exposure appears (> 500 L) to drive oxygen further into subsurface sites eventually forming an amorphous oxide layer that is stable to further doses. [Here, 1 langmuir (L)$\equiv 10^{-6}$ Torr sec.] There is, however, general disagreement as to the atomic surface structure at each stage of oxidation.

Theoretical electron band modeling of the oxidized layers hence relies on the experimental determination of density of states from techniques such as x-ray photoelectron spectroscopy (XPS), ultraviolet photoelectron spectroscopy (UPS), and angle-resolved ultraviolet photoelectron spectroscopy (ARUPS).[2] Our investigation utilizes symmetric transmission electron momentum spectroscopy (hereafter referred to as STEMS) to obtain direct information about the band structure of thin solid targets. This technique determines the initial state of a bound electron by measuring all kinematic variables related to an electron-induced ionizing reaction. Ritter et al.[3] have shown the value of this method on thin amorphous carbon foils, the momentum distributions clearly identifying and characterizing valence bands.

Previous STEMS studies have been carried out on aluminum–aluminum oxide in this laboratory[4] and by Persiantseva et al.[5] The poor efficiency of these experiments precluded energy resolutions better than 16 eV FWHM, which smoothed out valence-state details.

In this paper, an outline of STEMS is followed by a description of our preparation and characterization of thin (~ 100 Å) aluminum foil targets. The collected STEMS spectral momentum maps, covering binding energies from 0 to 40 eV and binding momenta -3.9 to 3.9 Å^{-1} with 4.5-eV FWHM and 1.1-Å^{-1} resolutions, respectively, are then presented and related to the foil's two-component composition, aluminum–aluminum oxide.

II. STEMS TECHNIQUE

A high-energy incident electron scatters from the target, knocking out a bound electron. These two outgoing electrons after being transmitted through the foil are then detected in coincidence, establishing they both originated from the same event. The energy and momentum of the incoming, scattered, and ejected electrons are $(E_i, \mathbf{k}_i)$, $(E_s, \mathbf{k}_s)$, and $(E_e, \mathbf{k}_e)$, respectively, as shown in Fig. 1. Defining the incident electron beam and detecting the two outgoing electrons at specific energies and angles, the
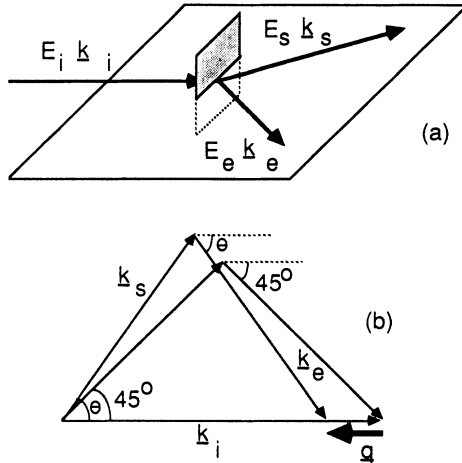
FIG. 1. (a) The incident, scattered, and ejected electrons have energies E_i, E_s, and E_e and momenta $\mathbf{k}_i$, $\mathbf{k}_s$, and $\mathbf{k}_e$, respectively, with the latter three vectors defining the coplanar scattering plane. (b) Momentum-conservation diagrams for symmetric scattering indicate how a change of scattering angle leads to different values of the binding electron momentum being measured.

momentum $\mathbf{q}$ and binding energy E_b of the precollision bound electron is simply determined by the conservation laws for energy,

$$E_b = E_i - (E_s + E_e) \ ,$$

and momentum,

$$\mathbf{q} = (\mathbf{k}_s + \mathbf{k}_e) - \mathbf{k}_i \ .$$

STEMS is able to pinpoint orbital and band states by measuring all kinematic variables related to a selected $(e,2e)$ reaction. For simple data interpretation we choose a geometry where all momenta are coplanar and the transmitted electrons are measured symmetrically about the beam direction, i.e., $\Theta_e = \Theta_S \approx 45°$ and $E_S = E_e \approx E_i/2$ (see Fig. 1). The target momentum is now found parallel to the incident beam and is

$$\mathbf{q} = (1 - \sqrt{2}\cos\theta_s)\mathbf{k}_i$$

$$\approx -(\pi/180°)\mathbf{k}_i \, \Delta\Theta \ ,$$

where $\Delta\Theta = \Theta_S - 45°$. Varying the analyzer's angle in unison enables $\mathbf{q}$ to be measured for a constant E_b.

The differential cross section for this $(e,2e)$ reaction is

$$\frac{d^3\sigma}{d\Omega_s \, d\Omega_e \, dE_s} = \frac{4\pi^3 k_s k_e}{k_0} \left[\frac{d\sigma}{d\Omega_s} \right]_{\text{Mott}} A(E_b,\mathbf{q}) \ ,$$

where $(d\sigma/d\Omega_s)_{\text{Mott}}$ is the Mott differential cross section for the scattering of two free electrons in the laboratory frame, which is approximately constant over the momentum range of interest at high energies employed. Thus, the coincident count rate is directly proportional to the spectral momentum density $A(E_b,\mathbf{q})$. This relationship has been verified in gas work[6] for beam energies of several keV.

For an ideal oriented single-crystal target an unambiguous band map complete with momentum densities could be found experimentally using this technique with appropriate energy and momentum resolutions. This map would be repeated with decreasing intensity of the spectral density at low order multiples of the reciprocal-lattice vector $\mathbf{K}$ such that $\mathbf{q} = \mathbf{q}_b + \mathbf{K}$ where $\mathbf{q}_b$ lies in the first Brillouin zone.

Polycrystalline targets represent an average over all lattice orientations when the crystallites are large on an atomic scale. This directional isotropy gives an average spectral momentum density $A(E_b,q)$. For simple "free-electron" systems such as aluminum which have a rotational symmetric band structure except near the Brillouin-zone boundaries, $A(E_b,q)$ is expected to be constant until it comes into contact with a zone boundary where it decreases by approximately a factor of 2. The spectral density falls quickly to zero for momentum larger than the Fermi momentum in the free-electron case.[7] Band dispersion of the parent crystal should be clearly reflected in $A(E_b,q)$ with bandwidths changing slightly for varying q. More complex foil targets with strongly anisotropic effective-mass tensors will produce spectral momentum densities that more smoothly decrease to zero beyond the Fermi momentum. As the foil becomes amorphous the band structure still resembles gross features of the crystalline solid. The band map close to the reciprocal-space origin is essentially the same, since the electron momentum envelope is comprised of long wavelengths and the solid structure on a large scale is unchanged. At larger k, local bond characteristics such as near-neighbor distances and angles become important, probably causing energy bands to broaden and the momentum density to drop smoothly to zero; see, for example, Ziman[8] and Mott.[9] The transition region in k depends on the type of solid-state electron scattering occurring. For weak scattering from phonons and impurities k remains a good quantum number, while the converse is true for small mean-free-path (L) strong processes, i.e., $kL \sim 1$, possibly creating localized Anderson states in the band-gap regions of suitable materials.

III. THE TARGET

Thin aluminum foils are prepared by rapid vacuum evaporation of 99.95%-pure aluminum from a electrically heated tungsten filament onto a soluble substrate at room temperature. The foils are separated in distilled water and then carefully mounted on target washers. Auger electron analysis of the target surface reveals a high degree of oxidation and carbon contamination, but no impurities are observed from the substrate. It is interesting to note that while raster scanning the target at 10 keV with a current of 10 nA under UHV conditions ($<10^{-9}$ torr) for ~ 5 min over a (0.2×0.2)-mm^2 area, a noticeable buckling occurred in the foil towards the probed area. Under an electron microscope (80-keV beam) the foil has a polycrystalline-amorphous character, with transmission electron diffraction patterns showing distinct fringes corresponding to the low-order Bragg directions of aluminum. The diffraction rings themselves reveal only slight

evidence of any preferred crystallite orientation within the target.

An approximate foil thickness is determined *in situ* by measuring the transmission energy-loss spectra at the straight-through position as shown in Fig. 2. It exhibits bulk-plasmon losses at multiples of 15.2 eV whose relative intensities are dependent on the path length and the electron's mean free path λ_p. Plasmon mean-free-path data were used from several sources, in particular Ishigure *et al.*,[10] who used a similar procedure for manufacturing aluminum foils. The foil thickness (t) can then be calculated assuming each plasmon loss is independent and applying Poisson statistics to the distribution

$$t = \frac{I_n}{I_{n+1}}(n+1)\lambda_p ,$$

where I_n is the area of the nth plasmon loss. Small corrections are made for the angular acceptance of the analyzers and the $\sim 10\%$ of nonindependent double plasmon losses. Targets are generally made self-supporting over a 2-mm hole for thicknesses between 80 and 140 Å to minimize multiple scattering in the coincident study. An estimated 15–30 Å saturated oxide layer on each face implies that the foils are equally divided between oxidized surfaces and bulk aluminum.

The energy-loss spectra in Fig. 2 confirm the high percentage of metallic aluminum by the presence of narrow, intense volume-plasmon losses. The less distinct surface-plasmon peak at 7 eV and a further broad volume plasmon at 22 eV correspond to the oxide-metal interface and oxide coating. The smooth underlying background results from inter- and intraband excitations in the two-component foil.

The vacuum system at pressures $\leq 10^{-8}$ torr plays an important role in the foil's characteristics under electron-beam bombardment. Initially it was found that with the vacuum system pumped by LN$_2$-trapped oil diffusion pump, with an Edwards 250-mm Diffstak, prolonged irradiation caused the total transmitted current to fall with time, and at 200 nA/mm^2 the current had a decay time of ~ 300 min. Similar behavior was reported by Ishigure.[10] The source of contamination was thought to

be carbon deposits formed by oil fractions cracking under the influence of the electron beam. The target lifetime was improved to several weeks by flushing the system with argon and using a 400 L s^{-1} ion pump instead of the diffusion pump, which maintained the pressure at 10^{-8} torr. The coincident data presented here were taken over several days and showed complete repeatability in that time.

IV. COLLECTED DATA

The measurement system utilizes a pair of two-dimensional position-sensitive microchannel-plate (MCP) assemblies to detect transmitted-energy-dispersed electrons from the slit outputs of two 180° hemispherical analyzers. This improves the efficiency by ~ 100 by gathering data over a band of energies in parallel, replacing the serial collection mode of one-channel detectors employing channeltrons. A more complete description of our multidimensional STEMS apparatus is given elsewhere.[11]

Initial experiments were performed on an extensively studied gas, argon, to characterize the linearity and sensitivity of the MCP's, to obtain an absolute energy scale, and to locate coincident windows in the time-to-amplitude converter (TAC) spectrum. In this case argon had many desirable properties, such as two well-separated states, $3p$ and $3s$, which could be accumulated simultaneously. From the coincidence binding-energy data on argon the experimentally determined energy resolution was 4.5 eV FWHM, with the MCP's acquiring data in parallel over a 50-eV range, as shown in Fig. 3. The origin of the energy scale is set by accepted positions of these states, eliminating contact potentials contributions of ~ 2.0 eV. An error of ± 1.5 eV is quoted to account for datum-point distances and nonlinearities in the MCP system which were $< 3\%$ full scale.

The argon-gas target was then replaced by rotating an aluminum foil into the interaction center, and repeating exactly the same procedure at various binding momenta.
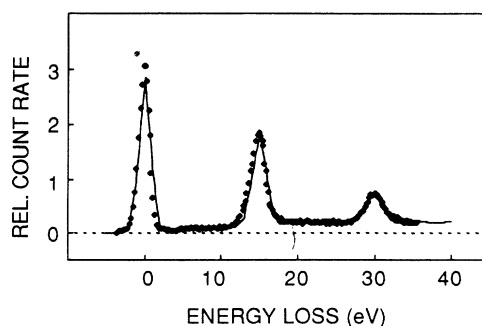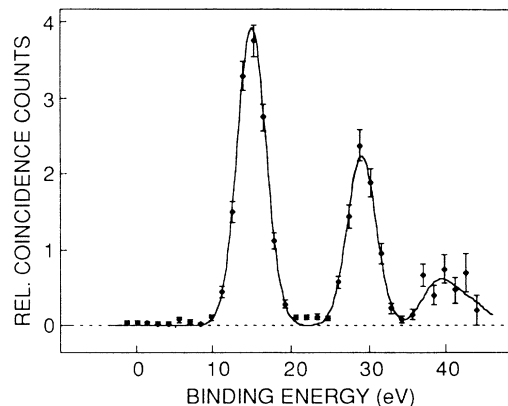

FIG. 2. Energy-loss spectrum ($\bullet$) for 3750-eV electrons transmitted through a 130-Å-thick foil at 0°. The line represents a Monte Carlo simulation of the loss processes with the foil.

FIG. 3. Coincidence binding-energy spectrum of argon gas using MCP data-collection system at 4.5-eV FWHM resolution. The line is a fit to the $3p$ and $3s$ ion state positions.

An electron-beam current of 150 nA gave a single-detector count rate of 20 kHz and a real total coincidence rate of 1.6 Hz at $q=0$ Å^{-1}. The random coincidence rate into the 4.7-ns-wide correlation timing window was 1.3 counts/sec. Charging of the foil was not a problem at this beam current, and reducing the current to 18 nA produced the same spectrum. Increasing the current, however, to 240 nA caused the spectrum to broaden and shift uniformly down in energy by 2.0 eV. The acquired raw spectral momentum map for the valence region of foil is shown in Fig. 4. Two distinct peaks are visible for $q=0$ Å^{-1}, located at energies $E_b=13$ and 31 eV. The second peak is sitting on a rising background, more clearly shown in Fig. 5 and discussed later. This extended coincidence binding-energy spectrum was produced by cyclically stepping the electron-beam voltage, overlapping individual energy sections.

The incident and escaping electrons belonging to a primary ionizing reaction can lose energy within the solid. These multiple-collision events constitute nearly all of the background. Creation of plasmons is the strongest mechanism, with mean free paths (MFP's) of order 100 Å. The separation of the peaks is 18 eV. With our electron energy resolution of 4.5 eV, the 15.2-eV aluminum-metal bulk-plasmon loss should significantly contribute to the broadening of the $(e,2e)$ energy-loss peaks. The different momentum distributions shown in Fig. 6, however, suggest that the second peak is not entirely a plasmon satellite of the first lower-energy state.

A simple Monte Carlo calculation for electrons traveling through a 130-Å foil coated with aluminum oxide 25 Å thick gave an estimate of the true intensity of the 31-eV state. The model allowed for energy losses in aluminum due to band excitation and surface- and bulk-plasmon creation, where the parameters are obtained

from Shimizu et al.,[12] Ishigure et al.,[10] Raether,[13] and our own measurement. The data for aluminum oxide were poor; mean free paths were found at higher energies from Swanson[14] and Leder[15] and then extrapolated back to our energies assuming it followed the same energy dependence as aluminum for bulk plasmons at 22 eV, 170-Å MFP's at 3.75 keV, and 250-Å MFP's at 7.5 keV. The parameters are most sensitive at the lower energy since the MFP's are shortest here and the two outgoing electrons are trying to escape the foil at 45° in the coincidence experiment at this energy. A check was performed by measuring the transmission energy-loss spectrum at 0° and running a simulation with the chosen parameter values. Figure 2 shows good agreement with only a small discrepancy at zero energy loss, which is probably due to electrons leaking through stress cracks around the supporting edge of the foil.

All small energy losses were assumed to cause only small-angle deflections in the electron's trajectory. The critical angle[13] for bulk aluminum plasmons at 3.75 keV is ~0.2°, which is inside the detector's angular resolution. Such collisions will smooth out the angular correlations. An escape-depth parameter was introduced to account for larger-angle deflections (essentially from elastic scattering) and absorption in the foil. For a coincidence event to be counted, both outgoing electrons have to emerge from the foil with shorter escape depths than the incoming electron. This constant weights the received coincident signal towards those ionization events occurring close to the exit surface of the foil. From Auger electron measurements[16] an escape depth at 3856 eV for aluminum oxide was found to be 22±3 Å including energy losses. Transmission current measurements (~5% transmitted) suggest a higher average escape depth of 40 Å at 3.75 keV and similarly one at (~12% transmitted)
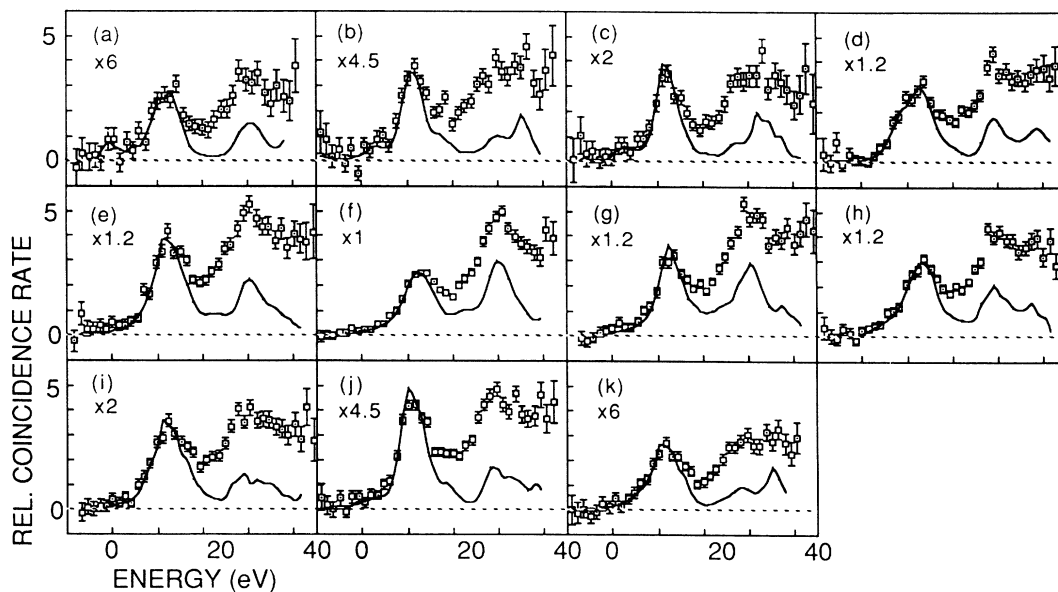

FIG. 4. Coincidence count rate vs electron binding energy at different binding momenta (in Å^{-1} units): (a) 3.9, (b) 3.1, (c) 2.3, (d) 1.5, (e) 0.77, (f) 0.0, (g) −0.77, (h) −1.5, (i) −2.3, (j) −3.1, and (k) 3.9. The lines on each plot are results of deconvolution of multiple-scattering background effects.
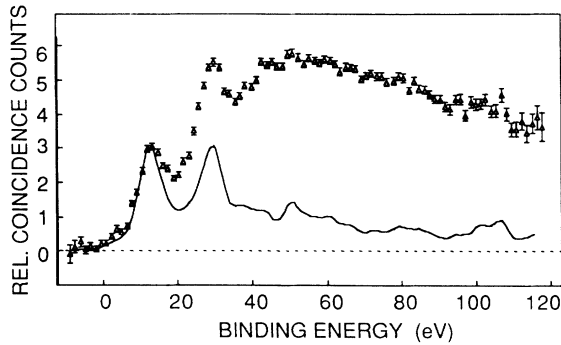
FIG. 5. Extended coincidence energy-loss spectrum for zero target-state momentum. The line represents the data with single-channel energy losses removed.
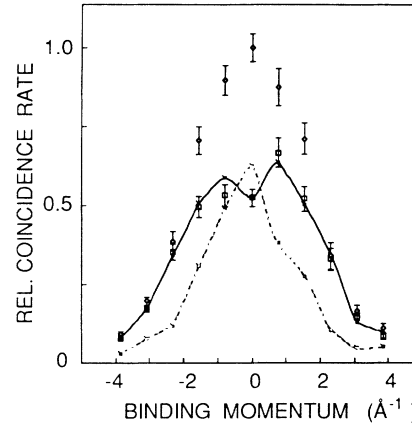

FIG. 6. Binding momentum spectra at (13 eV) (■) and 30-eV (◊) binding energies. Deconvoluting from the data the single-channel energy losses at 13 eV (——) and 30 eV (— — —) show more clearly the p and s character, respectively.

7.5 keV of 70 Å.

Applying the van Cittert method to deconvolute the simulated background from the extended coincidence energy-loss data of Fig. 5 yields two peaks of similar intensity located at 13 and 30 eV. At higher energies the intensity does not fall to zero, implying that MFP parameters have been overestimated. Part of the tail could be attributed to the coupling between the produced hole and the electron plasma, known as a plasmaron state.[17] There is only a slight, if any, indication of the $L_{2,3}$ state in aluminum–aluminum oxide at 82 eV.[18]

The same deconvolution procedure was applied to the binding momentum map (Fig. 4). Poor statistics at higher q and the small number of data points made an unambiguous extraction difficult. Both the data and the deconvoluted spectra in Fig. 6 show the first peak (13 eV) dropping at $q=0$ Å^{-1} with maxima at ± 0.77 Å^{-1}, while the second peak (30 eV) has its maximum at $q=0$ Å^{-1} decreasing symmetrically for higher-magnitude momenta. The interpretation that this structure predominantly belongs to aluminum oxide and not aluminum metal is the p-like nature of the first peak and the s character of the second. The smaller density of states for aluminum $3p$-$3s$ bands and the surface-sensitive nature of this technique should allow only minor contributions from 4 to 12 eV due to aluminum.

The energies of these states agree with the upper and lower valence bands of aluminum oxide, where hybridized O $2p$–Al $3p$ and O $2s$ orbital contributions, respectively, dominate the band's character, as shown by Ciraci et al.[19] and Balzarotti et al.[20] Both peaks show no statistically significant dispersion (≤ 1.0 eV across all bind-

ing momenta), consistent with the broad flat-band structure and the amorphous nature of the aluminum oxide. The lack of detail in the 13-eV peak probably illustrates the effects of local disorder near the surface, i.e., p-symmetry orbitals are generally involved in directional bonds which are more susceptible to defects. Poor statistics do not allow firm conclusions to be drawn about the gap between the two peaks. It does appear from Fig. 4 that the gap has a maximum intensity at $q=0$ Å^{-1} and decreases at higher magnitude q, and this change in intensity may indicate Anderson-localized states in between the two bands.

In conclusion, this experiment on aluminum–aluminum oxide thin films with STEMS has revealed two distinct states at 13 and 30 eV which we have attributed to the valence-band structure of oxide. Further work at better energy and momenta resolutions will continue on this metal-oxide thin foil to try and detail the band structure to a higher degree.

ACKNOWLEDGMENTS

[1] I. P. Batra and L. Kleinman, J. Electron. Spectrosc. Relat. Phenom. 33, 175 (1984).

[2] C. W. Martinson and S. A. Flödstrom, Solid State Commun. 30, 671 (1979).

[3] A. L. Ritter, J. R. Dennison, and R. Jones, Phys. Rev. Lett. 53, 2054 (1984).

[4] S. Dey, P. Hayes, and J. F. Williams, J. Phys. D 20, 504 (1987).

[5] N. M. Persiantseva, N. A. Krasilnikova, and V. G. Neudachin, Zh. Eksp. Teor. Fiz. 76, 1047 (1979) [Sov. Phys.—JETP 28, 540 (1979)].

[6] A. Lahmam-Bennani, H. F. Wellenstien, C. Dal Capello, M. Rousault, and A. Dugue, J. Phys. B 16, 2219 (1983).

[7] V. G. Levin, V. G. Neudachin, and Y. S. Smirnov, Phys. Status Solidi B 49, 48 (1972).

[8]J. M. Ziman, J. Phys. C **4**, 3129 (1971).

[9]N. F. Mott and E. A. Davis, *Electronic Processes in Noncrystalline Materials*, 2nd ed. (Clarendon, Oxford, 1979).

[10]N. Ishigure, Ce. Mori, and T. Watanabe, J. Phys. Soc. Jpn. **44**, 1196 (1978).

[11]P. Hayes, M. A. Bennett, J. Flexman, and J. F. Williams, Rev. Sci. Instrum. (in press).

[12]R. Shimizu, Y. Kataoka, T. Ikuta, T. Koshikawa, and H. Hashimoto, J. Phys. D **9**, 101 (1978).

[13]H. Raether, *Excitation of Plasmons and Interband Transitions by Electrons*, Vol. 88 of *Springer Tracts in Modern Physics*, edited by G. Höhler (Springer-Verlag, Berlin, 1980).

[14]N. Swanson, Phys. Rev. **165**, 1067 (1968).

[15]L. B. Leder, Phys. Rev. **101**, 1721 (1956).

[16]M. Klasson, J. Hedman, A. Bernotsson, R. Nilsson, and C. Nordling, Phys. Scr. **5**, 93 (1972).

[17]B. I. Lundquist, Phys. Condens. Matter **6**, 193 (1967).

[18]P. H. Citrin, J. E. Rowe, and S. B. Christman, Phys. Rev. **16**, 2642 (1976).

[19]S. Ciraci and I. P. Batra, Phys. Rev. B **28**, 982 (1983).

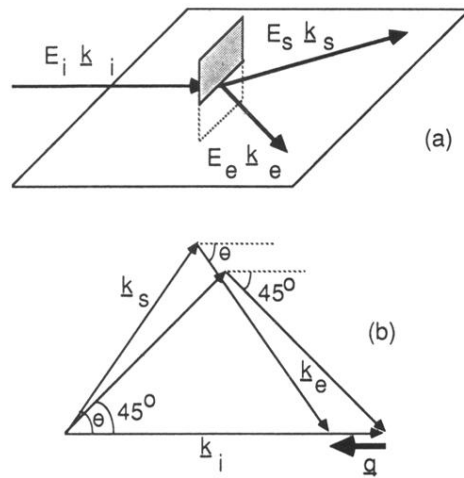[20]A. Balzarotti and A. Biaconi, Phys. Status Solidi B **76**, 689 (1976).

FIG. 1. (a) The incident, scattered, and ejected electrons have energies E_i, E_s, and E_e and momenta $\mathbf{k}_i$, $\mathbf{k}_s$, and $\mathbf{k}_e$, respectively, with the latter three vectors defining the coplanar scattering plane. (b) Momentum-conservation diagrams for symmetric scattering indicate how a change of scattering angle leads to different values of the binding electron momentum being measured.